Self-similar, surfactant-driven flows

O. E. Jensen
Department of Mathematics and Statistics, University of Newcastle upon Tyne, Newcastle upon Tyne, NE1 7RU, England

(Received 11 May 1993; accepted 15 November 1993)

Consider a dilute, insoluble surfactant monolayer on the free surface of a thin viscous film. A gradient in surfactant concentration generates a gradient in surface tension, driving a flow that redistributes the surfactant so that these gradients decay. The nonlinear evolution equations governing such flows, derived using lubrication theory, have previously been shown to admit a set of simple similarity solutions representing the spreading of a monolayer over an uncontaminated interface. Here, a much more general class of similarity solutions is considered, and a transformation is identified reducing the governing partial differential equations to a set of nonlinear ordinary differential equations, the solutions of which correspond to integral curves in a two-dimensional phase plane. This allows the construction of solutions to a wide range of problems. Many new solutions are revealed, including one that cannot be determined by simpler techniques, namely the closing of an axisymmetric hole in a monolayer, the radius of which is shown to be proportional to $(-t)^{\delta}$ as $t \to 0-$, where $\delta \approx 0.807\,41$; this solution corresponds to a heteroclinic orbit in the phase plane.

I. INTRODUCTION

A spatially localized surfactant monolayer lying on the free surface of a layer of liquid is self-spreading. This is because interfacial surface tension is a diminishing function of local surface concentration of surfactant, and so a nonuniform distribution of surfactant generates gradients in surface tension, and thus shear stresses, which drive a flow that tends to diminish concentration gradients. If the liquid layer is thin, and if the monolayer lies on an otherwise uncontaminated interface, this flow produces substantial deformation of the free surface of the liquid layer. Provided surface diffusion and gravitational forces are weak, a large gradient in shear stress develops at the leading edge of the monolayer, which gives rise to an advancing shock-like discontinuity in liquid layer depth.[1] Film elevation behind the shock necessitates severe thinning of the layer nearer the center of the monolayer,[2,3] which may be sufficient to initiate film rupture.[4,5] Surfactant solubility can either enhance[6] or diminish[7] such film deformations, depending on the conditions.

Flows generated by gradients in surfactant concentration are of particular interest because of the important role played by surfactant in the lung. All the air spaces in the lung are lined with a thin layer of fluid, and the lung produces a natural surfactant to minimize the potentially harmful effects of high surface tension at the free surface of this liquid layer. The lungs of prematurely born infants are insufficiently mature to produce their own surfactant, and so a substitute may be delivered to them artificially, either by direct instillation or as an inhaled aerosol. In either case, the self-spreading property of surfactant monolayers is potentially a significant factor in the success of these clinical techniques. Surfactant-driven flows also arise naturally in the terminal bronchioles, where a gradient in surfactant concentration is maintained between the alveoli (where surfactant is produced) and the airways to which they are connected. The resulting flows serve as a waste-disposal system, carrying waste up to the larger, ciliated airways. Flows driven by surfactant gradients also have industrial applications: surfactant inhomogeneities may induce surface defects in drying paint films,[8] while Marangoni effects can be harnessed to enhance other drying processes.[9]

The behavior of a dilute, insoluble surfactant monolayer on a thin liquid film may be modeled using lubrication theory, from which a pair of coupled nonlinear evolution equations for the film height h and the surfactant concentration Γ are derived. Equation (1), for example, describes flows generated by gradients in surface tension alone: the effects of surface diffusion, gravity, and the mean interfacial surface tension are neglected, an approximation that is realistic for flows of many surfactants on sufficiently thin liquid layers, and most flows in the lung, in particular. These equations have previously been shown to admit steady solutions[10] describing flows related to those down terminal bronchioles, a traveling-wave solution[1] describing a monolayer pushed along by a steadily translating barrier, and a set of similarity solutions[5,11] describing the spreading of a localized monolayer. The purpose of this paper is to show that these examples fall into a much wider class of similarity solutions of (1), a number of which describe novel surface-tension-driven flows, some having direct pulmonary applications.

This is achieved by identifying a transformation of (1) to a set of three ordinary differential equations [(6) and (8)]. Fortunately, one of these is uncoupled from the other

 1070-6631/94/6(3)/1084/11/$6.00

two, allowing solutions to be represented as trajectories in a two-dimensional phase plane. The nature of each plane is determined by parameters related to the geometry of the problem and the respective strengths of sources of fluid and surfactant. Each trajectory represents a similarity solution satisfying particular initial or boundary conditions. Only a very small subset of trajectories are of significant interest, however, and so for brevity only these will be considered here. Nevertheless, this method provides a systematic way of determining all similarity solutions of (1) that are of a specific, but quite general, form. In this it follows a number of studies, from early investigations of compressible flows[12] to recent studies of viscous gravity currents[13,14] (see these papers for further references). This technique has also been applied to a class of nonlinear diffusion equations,[15,16] of which the equation describing a viscous gravity current is a member. Here, it will be shown that despite being of higher order, the coupled equations (1) exhibit many characteristics of the viscous-gravity-current problem.

A common feature of the self-similar surfactant-driven flows described previously[5,11] is that they can all be derived through simple physical arguments, involving the conservation of a globally conserved quantity (e.g., the total quantity of surfactant in a monolayer), and as a result the flows are governed by relationships such as "monolayer length $\propto t^{\delta}$," where δ is a simple fraction. As such, these are typical so-called "similarity solutions of the first kind."[17] The most significant advantage of the phase-plane method described here is that it enables one to identify similarity solutions "of the second kind," i.e., solutions that cannot be derived by physical balances alone, typically because they fail to satisfy a global constraint: the condition used to determine such a solution is that of its mathematical existence, and so δ becomes the solution of a nonlinear eigenvalue problem, making it (in general) transcendental. An example of a "second-kind" solution is presented below, describing the final stages of the closing of an axisymmetric hole in a monolayer; it is represented by a heteroclinic orbit in the phase plane, which exists for a unique value of δ. The prediction that the hole's diameter diminishes approximately proportionally to $(-t)^{0.807\,41}$ as $t\to 0-$ is shown to agree well with numerical solutions of the fully time-dependent equations (1).

II. THE GOVERNING EQUATIONS

The model corresponds very closely to that described elsewhere,[1,2,5] and so only a brief outline is necessary. A layer of incompressible, Newtonian fluid of viscosity μ and undisturbed thickness H_0 lies on a flat, horizontal plane. On its surface a dilute, insoluble surfactant monolayer is present. The concentration of the monolayer Γ^* determines the local surface tension of the film through an equation of state, which, for sufficiently small Γ^*, may be assumed to be linear, so that $\Delta\sigma^* = -A\,\Delta\Gamma^*$, where $A(>0)$ measures the "activity" of the surfactant when dilute and Δ represents a small variation in a quantity. Gradients in Γ^* occurring over a long horizontal length scale of $O(H_0/\epsilon)$, where $\epsilon \ll 1$ give rise to gradients in σ^*, and thus to shear stresses at the free surface of the liquid layer of $O(\epsilon S/H_0)$, where S is a typical magnitude of $\Delta\sigma^*(S=A\Gamma_0$, where Γ_0 is a typical concentration). A flow is generated with a velocity of order $U_0=\epsilon S/\mu$. We assume that the liquid layer is sufficiently thin for gravitational forces to be negligible (i.e., $\rho g H_0^2/S \ll 1$, where ρ is the density of the liquid layer and g the acceleration due to gravity), for inertial effects to be negligible (which requires $\epsilon^2\,\mathrm{Re} \ll 1$ where $\mathrm{Re}=\rho H_0 S/\mu^2$), and that the mean surface tension σ_0 of the film is negligible [which holds for $\sigma_0=O(S)$]. This being the case, and provided spatial gradients in film height remain $O(1)$, there are no pressure gradients in the fluid layer at leading order, and the flow is driven entirely by shear stresses. Situations when gradients in film height are very large will be discussed as they arise in what follows.

For reference, typical orders of magnitude of these parameters are $g\sim 10^3$ cm/s^2, $\rho\sim 1$ g/cm^3, $S\sim\sigma_0\sim 10$ dyn/cm, $\epsilon\sim 10^{-2}$, and $H\sim 1$ mm, $\mu\sim 10^{-1}$ g/(cm s) in experiment,[4] or $H\sim 10^{-4}$ cm, $\mu\sim 10^{-2}$ g/(cm s) in a lung alveolus. In both cases the surface diffusivity of surfactant D_s is of order 10^{-5} cm^2/s. Thus, U_0, $\rho g H_0^2/S$, $\epsilon^2\,\mathrm{Re}$, and the nondimensional surface diffusivity $\mathscr{D}=\epsilon D_s/U_0 H_0$ (the inverse surface Péclet number) are, respectively, of order 1 cm/s, 1, 10^{-2}, 10^{-6} in an experiment and 10 cm/s, and 10^{-6}, 10^{-3}, 10^{-4} in an alveolus. Surface diffusion of surfactant will therefore be neglected in much of the following analysis.

The following nondimensional variables can now be introduced: coordinates x and z parallel and normal to the wall beneath the fluid layer; time t; the layer thickness $h(x,t)$; the surfactant monolayer concentration $\Gamma(x,t)$; the component of surface tension that varies with Γ, namely, $\sigma(x,t)$; and the horizontal velocity in the fluid layer $u(x,z,t)$ (these are scaled on H_0/ϵ, H_0, $H_0/\epsilon U_0$, H_0, Γ_0, S, and U_0, respectively). Using the lubrication-theory approximation, the horizontal momentum equation at leading order in ϵ is $u_{zz}=0$. Applying the no-slip condition at $z=0$ and the tangential stress boundary condition at $z=h$, it follows that the horizontal velocity in the fluid layer is $u(x,z,t)=\sigma_x z$, where $\sigma_x=-\Gamma_x$. Substituting this expression into the depth-integrated mass conservation equation for the fluid and into the transport equation for surfactant gives the following pair of coupled nonlinear evolution equations:

$$\left.\begin{aligned} &h_t+\frac{1}{2x^n}\,(x^n h v)_x=0,\\ &\Gamma_t+\frac{1}{x^n}\,(x^n\Gamma v)_x=0, \end{aligned}\right\} \quad \text{where } v+h\Gamma_x=0. \tag{1}$$

Here, $v(x,t)$ is the velocity at the free surface of the liquid layer. For a planar geometry $n=0$; for an axisymmetric geometry $n=1$. Nonintegral values of n can also be considered: these correspond to a monolayer on the free surface of a liquid layer that lines a tube, where the tube's circumference varies with the axial distance down the tube proportionally to x^n. The curvature of the tube has negligible effect, provided the liquid layer is sufficiently thin.

III. THE TRANSFORMATION

To transform (1) to a similarity form, we exploit some of the symmetries of the equations. Clearly, v scales like x/t and $h\Gamma$ like x^2/t, suggesting that the dependent variables be reexpressed as

$$h(x,t)=\left(\frac{x^2}{t}\right)^{\alpha}\hat{h}(x,t),\quad \Gamma(x,t)=\left(\frac{x^2}{t}\right)^{(1-\alpha)}\hat{\Gamma}(x,t),$$
$$v(x,t)=\left(\frac{x}{t}\right)\hat{v}(x,t), \tag{2}$$

where $\alpha\geqslant 0$ is a constant and $t>0$. If $t<0$, we use instead $h(x,t)=[x^2/(-t)]^{\alpha}\hat{h}(x,t)$, $\Gamma(x,t)=-[x^2/(-t)]^{(1-\alpha)}\hat{\Gamma}(x,t)$. This turns (1) into a form that is homogeneous in x and t:

$$2t\hat{h}_t-2\alpha\hat{h}+x(\hat{h}\hat{v})_x+(n+2\alpha+1)\hat{h}\hat{v}=0,$$
$$t\hat{\Gamma}_t-(1-\alpha)\hat{\Gamma}+x(\hat{\Gamma}\hat{v})_x+[n+2(1-\alpha)+1]\hat{\Gamma}\hat{v}=0, \tag{3}$$
$$\hat{v}+2(1-\alpha)\hat{h}\hat{\Gamma}+x\hat{h}\hat{\Gamma}_x=0.$$

We now make the assumption that for $t>0$, x and t arise in the combination $\xi=x/t^{\delta}$, for some constant δ [likewise $\xi=-x/(-t)^{\delta}$ if $t<0$]. Further, (3) can be made autonomous if the new independent variable is chosen as $\phi=\log|\xi|$ (so solutions are invariant under a rescaling of ξ). Then, writing

$$\hat{h}(x,t)=H(\phi),\quad \hat{\Gamma}(x,t)=G(\phi),\quad \hat{v}(x,t)=V(\phi), \tag{4}$$

(3) becomes

$$H_{\phi}(V-2\delta)+HV_{\phi}-2\alpha H+(n+2\alpha+1)HV=0, \tag{5a}$$
$$G_{\phi}(V-\delta)+GV_{\phi}-(1-\alpha)G+[n+2(1-\alpha)+1]GV=0, \tag{5b}$$
$$V+2(1-\alpha)HG+HG_{\phi}=0. \tag{5c}$$

We can now take advantage of the fact that (5) is invariant under a scaling that preserves the product HG, by introducing this product as a dependent variable, $U(\phi)$, say. Once H has been replaced by U/G in (5), G arises only in the combination G_{ϕ}/G, making it natural to introduce a new variable $\psi=\log|G|$, which takes account the invariance of the resulting equations under a rescaling of G. Then, using (5c) to eliminate ψ_{ϕ}, (5a) and (5b) can be rearranged to give

$$\frac{dU}{d\phi}=-\left(\frac{U[2V+1-6\delta-3\alpha(1-2\delta)]+V(2V-3\delta)}{(V-2\delta)}\right), \tag{6a}$$

$$\frac{dV}{d\phi}=-\left(\frac{U[(n+1)V+(2\delta-1)(1-\alpha)]+V(\delta-V)}{U}\right). \tag{6b}$$

Solutions of (6) may be represented as trajectories in the (U,V)-phase plane, which are integral curves satisfying

$$\frac{dV}{dU}=\frac{(V-2\delta)}{U}\left(\frac{U[(n+1)V+(2\delta-1)(1-\alpha)]+V(\delta-V)}{U[2V+1-6\delta-3\alpha(1-2\delta)]+V(2V-3\delta)}\right). \tag{7}$$

The trajectories may be parametrized either by ϕ or by ψ, where (from 5c)

$$\frac{d\psi}{d\phi}=-\left(\frac{V+2(1-\alpha)U}{U}\right). \tag{8}$$

Thus, given a trajectory $[U(\phi),V(\phi)]$, the corresponding physical solution is recovered through integration of (8) to determine $\psi=\psi(\phi)$, and thus $\xi=e^{\phi}$, $G=e^{\psi(\phi)}$, and $H=U/G$, and hence h and Γ.

A phase plane is fully specified by three parameters, n, α, and δ, and so a wide range of planes are possible. Further, each trajectory in each plane represents a different solution, putting a full classification of all solutions beyond the scope of this paper. Instead, we shall concentrate on a few carefully chosen values of the parameters, ignoring a wide (but largely physically uninteresting) range of solutions, remarking that a framework now exists for their investigation, should this prove of value. The geometrical parameter will therefore be taken to be $n=0$ or $n=1$. The parameter α is related to the total mass of fluid in the system; we concentrate on the case $\alpha=0$, although other values are potentially of interest if a source or sink of fluid exists. The parameter δ, a measure of the rate of spreading (with t positive and increasing) or contraction (with t negative and increasing) of a monolayer, can be controlled by a source or sink of surfactant. We restrict attention almost exclusively to $0\leqslant\delta\leqslant 1$: in the limit $\delta=0$ we recover quasisteady solutions of (1); the limit $\delta=1$ corresponds to traveling-wave solutions.

Henceforth, therefore, we put $\alpha=0$. The total quantity of surfactant in the monolayer, $(2\pi)^n\int_0^{\infty}x^n\Gamma dx$, is then proportional to $t^{(n+3)\delta-1}=t^p$, say. A spreading monolayer constituting a fixed amount of surfactant corresponds to $p=0$, i.e., $\delta=1/(n+3)$, and hence we recover the scalings for a spreading planar monolayer "strip" ($n=0$) and for an axisymmetric monolayer disk or "drop" ($n=1$), which advance like $t^{1/3}$ and $t^{1/4}$, respectively,[5,11] (we follow the terminology used in Ref. 5). The other scaling we can identify immediately is that of a monolayer fed from a source at which Γ is held constant: since Γ is proportional to x^2/t in (2), the only way for Γ to be independent of t as $x\to 0$ is to have $\delta=\frac{1}{2}$. Thus, a planar or an axisymmetric monolayer fed from such a source spreads like $t^{1/2}$, and corresponds to $p=\frac{1}{2}$ (if $n=0$, the "front" case in Ref. 5)

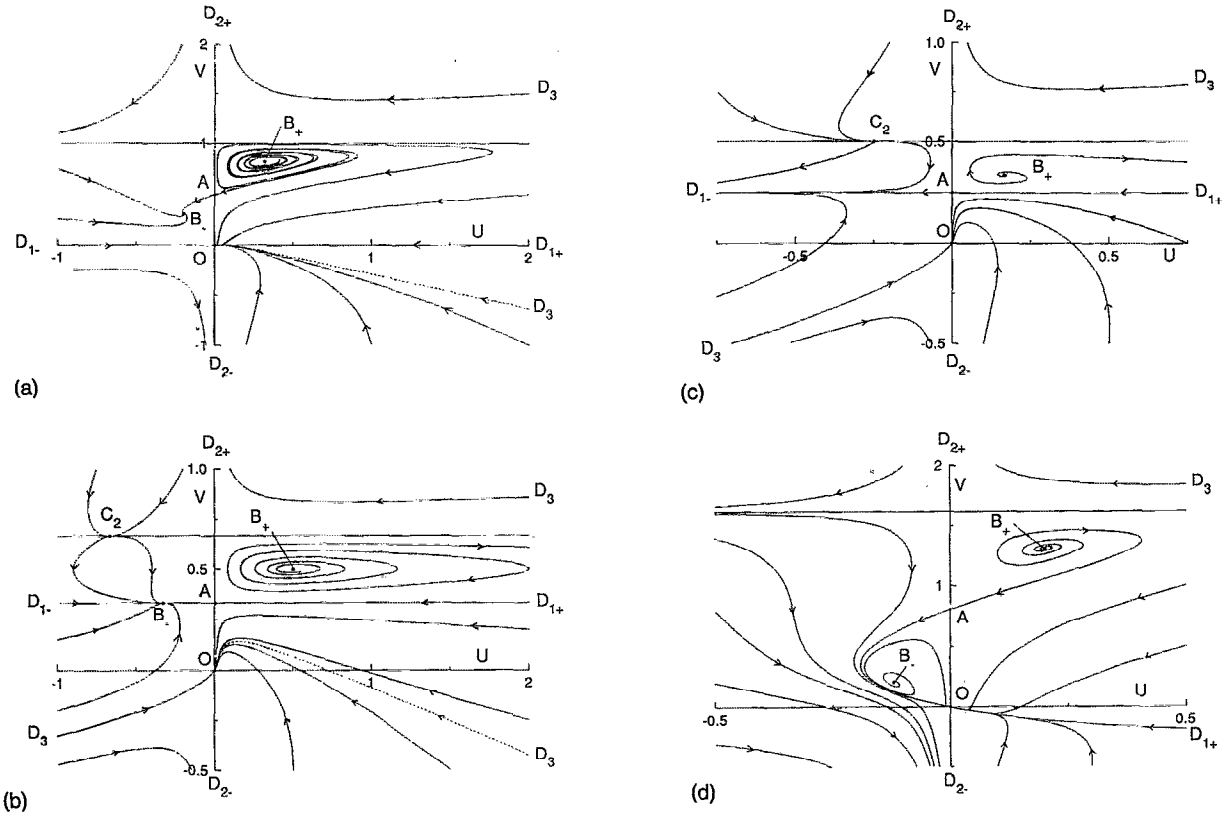

FIG. 1. The (U,V) phase plane. Arrows indicate the direction of increasing ϕ. (a) $n=0$, $\delta=\frac{1}{2}$: B_+A0 represents a planar "front" advancing over an uncontaminated film; the dotted line is the separatrix from D_3. (b) $n=0$, $\delta=\frac{1}{3}$: $D_{1+}AO$ represents the spreading "strip" solution. (c) $n=1$, $\delta=\frac{1}{4}$: $D_{1+}AO$ represents the spreading "drop" solution; in this case B_- is coincident with $D_{1\pm}$. (d) $n=1$, $\delta=0.807\,41$: the heteroclinic orbit AO represents a closing axisymmetric hole in a monolayer.

and $p=1$ (if $n=1$). The phase planes can now be used to identify *all* solutions sharing these particular scalings, as well as new solutions for other values of δ.

IV. THE PHASE PLANE

Four different (U,V)-phase planes are shown in Fig. 1. These do not give a complete picture of possible behavior, but are cases of specific interest and will be used to illustrate the following discussion. The corresponding parameter values are Fig. 1(a), $n=0$, $\delta=\frac{1}{2}$, the "front" scaling; Fig. 1(b), $n=0$, $\delta=\frac{1}{3}$, the "strip" scaling; Fig. 1(c), $n=1$, $\delta=\frac{1}{4}$, the "drop" scaling; and Fig. 1(d), $n=1$, $\delta=0.807\,41$, almost exactly the "closing hole" scaling. In this section we assume that $\alpha=0$ and $\delta>0$; the case $\delta=0$ is discussed in Sec. V D below.

Two obvious physical constraints are $h\geqslant 0$ and $\Gamma\geqslant 0$. Since $U=(h\Gamma)t/x^2$, $U>0$ therefore corresponds to $t>0$ (spreading distributions) and $U<0$ to $t<0$ (contracting distributions). Likewise, since $v=(x/t)V$, the quadrants of the phase plane correspond to the following: if $U>0$, $V>0$ ($V<0$) represents outward (inward) velocities; if $U<0$, $V>0$ ($V<0$) represents inward (outward) velocities.

Two trajectories are evident immediately from (7), the lines $V=2\delta$ and $U=0$. Along the former $d\phi/dU=0$, along the latter $d\phi/dV=0$, i.e., the parametrization of trajectories by ϕ is singular. The arrows on the trajectories in Fig. 1 show the direction of increasing ϕ, and so they change direction across both lines (except at singular points). Along $U=0$, the velocity V can change at fixed ϕ, i.e., V can be a discontinuous function of position. This corresponds, for example, to the conditions at the shock at the leading edge of the monolayer,[1] at which $G=0$, and so $U=0$.

The physical significance of the remaining trajectories is best described by considering the fixed points of (7), in turn, and the corresponding asymptotic forms of h and Γ that each represents. For brevity, the derivation of the asymptotic results is not described, and any arbitrary constants that arise are set to unity, since it is only the algebraic dependence of h and Γ on x and t that is of interest at this stage. Each fixed point is indicated on Fig. 1, where appropriate.

(1) *Point O, at* (0,0), *representing* $|x|\to\infty$. For $\delta>0$, the origin is an attracting node in $U>0$, and a saddle in $U<0$. In $U>0$ all trajectories approach the line $(2\delta-1)U+\delta V=0$ [e.g., the line $V=0$ in Fig. 1(a)], which is also tangential to the separatrix in $U<0$. Points along this line represent solutions satisfying $h\sim$const and $\Gamma\sim|x|^{(2-1/\delta)}$ as $|x|\to\infty$, so that *all* the trajectories in Fig. 1(a) approaching the origin in $U>0$ satisfy a physically realistic boundary condition: these are considered in more detail in Sec. V A below. The separatrix from O is of interest in the special cases in which it connects with the saddle point A; this occurs for $\delta=\delta_c$, where $\delta_c=1$ $(n=0)$ and

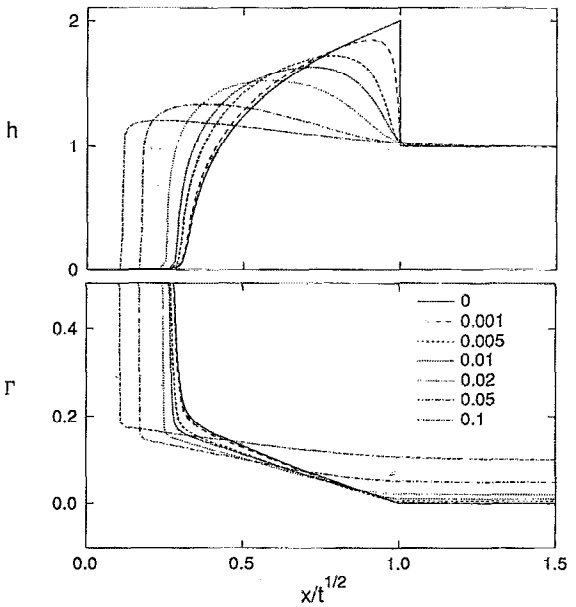

FIG. 2. Advancing monolayers in the case $n=0$, $\delta=\frac{1}{2}$. The solid line corresponds to the trajectory B_+AO in Fig. 1; the remaining lines to trajectories B_+O. The value of Γ as $x\to\infty$ is indicated in the lower panel.

$\delta_c\approx 0.807\,41$ ($n=1$), the case shown in Fig. 1(d).

(2) *Point A, at* $(0,\delta)$, *representing* $x=t^\delta$. For $\delta>0$, A is a saddle. One separatrix is the V axis, along which v can change discontinuously as a function of position, as it does at the shock at the leading edge of the monolayer. The other separatrix is tangential to the line $V=\delta+U[(n+3)\delta-1]/(2\delta)$. When $(n+3)\delta-1=0$, i.e., exactly the situation $p=0$ described in Sec. III representing a spreading "strip" or "drop," the line $V=\delta$ is a trajectory of (7); see Figs. 1(b) and 1(c). In general, the segment of the separatrix in $U>0$ ($U<0$) represents the behavior of the film upstream of a spreading (contracting) shock at $x=t^\delta$. As $x\to t^\delta-$ for $t>0$, $h\sim$const and $\Gamma\sim t^{(2\delta-1)}(1-x/t^\delta)$. The trajectories B_+AO in Fig. 1(a), $D_{1+}AO$ in Figs. 1(b) and (c) therefore correspond, respectively, to the "front," "strip," and "drop" solutions of Ref. 5 (see Sec. V A and Fig. 2).

(3) *Points* B_+ *and* B_-, *at* $(U_\pm, V_\pm)$, *representing* $|x|\to 0$ *or* $|x|\to\infty$. The two nontrivial fixed points of (7) at $(U_\pm, V_\pm)$, given by

$$U_\pm=\frac{1-7\delta+14\delta^2+n\delta(6\delta-5)\pm(1+2\delta)\Theta}{4(2+n)[-3+10\delta+n(6\delta-1)]},$$
$$V_\pm=\frac{1+7\delta+3\delta n\pm\Theta}{4(2+n)}, \tag{9}$$

where

$$\Theta=\sqrt{1-18\delta+49\delta^2-10\delta n+42\delta^2 n+9\delta^2 n^2}, \tag{10}$$

exhibit quite complex behavior, but only a summary of the relevant details need to be given here. Both points exist provided $\Theta\geqslant 0$, i.e., for $\delta\leqslant\delta_-$ and $\delta_+\leqslant\delta$, where $0<\delta_-<\delta_+<1$. At these critical values of δ the points coalesce in saddle–node bifurcations. The point B_- is coincident with O if $\delta=0$, otherwise $V_\pm>0$ when $B_\pm$ exist. For $0<\delta\leqslant\delta_-$, B_- and B_+ occur as a saddle–node pair, respectively, in $U<0$, both lying above the line $2U+V=0$.

If $n=0$, then $\delta_\pm=(9\pm 2^{5/2})/49$. At $\delta=\delta_+\approx 0.2991$, B_+ and B_- are created as a saddle–node pair, respectively, in $U<0$; as δ is increased B_+ moves rapidly away to $(-\infty,\frac{2}{5})$ as $\delta\to\frac{3}{10}-$, and then reappears as attracting fixed point from $(+\infty,\frac{2}{5})$ for $\delta=\frac{3}{10}+$, and $U_+>0$ thereafter; B_- remains as an attracting fixed point in $U<0$. At $\delta\approx 0.318$, B_+ changes stability and sheds a stable limit cycle, which is destroyed at a heteroclinic bifurcation involving A and D_{1+} at $\delta=\frac{1}{3}$ [shown in Fig. 1(b)]. Note that for $\delta\to\frac{1}{3}-$ the A separatrix in $U>0$ originates from D_3 (defined below), and that from D_{1+} approaches the stable limit cycle around B_+; for $\delta\to\frac{1}{3}+$, the A separatrix connects with B_+ and the D_{1+} separatrix with O, as in Fig. 1(a). For $\delta>\frac{1}{3}$, B_+ is an unstable focus [e.g. Fig. 1(a)], until $\delta\approx 0.65$ when it sheds an unstable limit cycle, which is destroyed in another heteroclinic bifurcation involving A and C_{2+} (defined below) at $\delta=1$. The heteroclinic trajectory is the curve $U=V(V-1)$ (representing an exact solution; see Sec. V B), which also connects the separatrices of A and O in $U<0$ [so that here it resembles Fig. 1(d)]. The segment in $U<0$ gives birth to an unstable limit cycle encircling B_- as δ is increased from 1; this limit cycle vanishes in a Hopf bifurcation at $\delta\approx 1.16$.

If $n=1$, then $\delta_\pm=(7\pm 24^{1/2})/50$, and the coalescence of B_+ and B_- at $\delta=\delta_+$ occurs in $U>0$; as δ is increased from $\delta_+\approx 0.238$ toward $\frac{1}{4}$, B_- (a saddle) moves rapidly away to $(\infty,\frac{1}{4})$. Figure 1(c) shows the phase plane when $\delta=\frac{1}{4}$. Then B_- reappears from $(-\infty,\frac{1}{4})$ for $\delta=\frac{1}{4}+$ as an attracting point, and stays in $U<0$ thereafter. Here B_+ remains as a repelling point for $\delta>\delta_+$ in $U>0$ [e.g., Figs. 1(c) and 1(d)]. In addition, B_- changes stability at $\delta\approx 0.94$, absorbing an unstable limit cycle, previously created in a heteroclinic bifurcation involving the separatrices of O and A at $\delta=\delta_c\approx 0.807\,41$, shown in Fig. 1(d). Note for $\delta<\delta_c$ the separatrices from O and A connect with D_3 and B_-, respectively [as in Fig. 1(c)]; for $\delta>\delta_c$ they connect with the limit cycle around B_- and D_{2-}, respectively.

The fixed points $B_\pm$ represent the limit $|x|\to 0$ when repelling and $|x|\to\infty$ when attracting. At leading order, (6) and (8) imply that for finite $U_\pm$, $h\sim(xt^{-\delta})^{2+\lambda_\pm}$, $\Gamma\sim(xt^{-\delta})^{-\lambda_\pm}t^{(2\delta-1)}$, where $\lambda_\pm=V_\pm/U_\pm$. In most cases of interest, B_+ (B_-) is a repelling (attracting) point for which $\lambda_+>0(\lambda_-<0)$, and so $\Gamma\to\infty$ as $|x|\to 0(|x|\to\infty)$ [e.g., Fig. 1(a)]. Similarly, $2+\lambda_\pm>0$ for $n=0$, $\delta>\delta_+$, and for $n=1$, $\delta>\frac{1}{4}$, so that $h\to 0$ in both limits. When $n=1$ and $\delta=\frac{1}{4}$, U_- is infinite and the spreading "drop" solution, represented by the trajectory $D_{1+}AO$ in Fig. 1(c) and given explicitly in (15) below also has Γ unbounded and $h\to 0$ as $|x|\to 0$. (These unrealistic boundary conditions are not realized in practice;[5] see Sec. V A.)

(4) *Point* $D_{1\pm}$, *at* $[\pm\infty,(1-2\delta)/(n+1)]$, *representing* $|x|\to 0$. This point is reached along a separatrix that is parallel to $V=(1-2\delta)/(n+1)$ as $|U|\to\infty$. It corresponds to the limit $|x|\to 0$, where $h\sim(xt^{-\delta})^c$ and $\Gamma\sim t^{(2\delta-1)}$, with

$$c=\frac{(n+1)(1-2\delta)}{2\delta(n+2)-1}. \tag{11}$$

The case in which $c=2$, $\delta=\frac{1}{2}(n+3)/(3n+5)$, corresponds to the situation in which D_1 is coincident with either B_+ if $n=0$ ($\delta=\frac{3}{10}$) or with B_- if $n=1$ [$\delta=\frac{1}{4}$, shown in Fig. 1(c)]. Otherwise, D_1 is a saddle (except when coincident with $V=2\delta$). Under the conditions of Fig. 1(b), $c=1$, which corresponds to the "strip" solution (14) below with h linear in x. When $\delta=\frac{1}{2}$, $c=0$ and D_1 lies on $V=0$ [Fig. 1(a)]; this line is a trajectory, representing constant h and Γ.

(5) *Point* $D_{2\pm}$, *at* $(0,\pm\infty)$, *representing* $x=t^\delta$. This point is a node, attracting if $UV>0$ and repelling if $UV<0$. It corresponds to behavior at a point $x=t^\delta$. Trajectories in $U>0$ approaching $D_{2\pm}$ represent the limit $x\to t^\delta\mp$, respectively. In the limit $x\to t^\delta-$, say, the combinations h/Γ and hv tend to a constant, with $h\sim(1-x/t^\delta)^{1/3}$. Thus both h and Γ tend to zero, while v becomes infinite. This corresponds to the draining of a flow off a finite plate whose edge is at $x=t^\delta$, either expanding or contracting, depending on the sign of t. This is a direct analog of the solutions described by Gratton and Minotti, representing the flow of a viscous gravity current off a finite plate.[13] Likewise, trajectories originating from D_{2-} [e.g., trajectories $D_{2-}O$ in Fig. 1(a)] describe the flow draining off a semi-infinite plate lying in $x>t^\delta$. These solutions can be readily generalized to include a source or sink of fluid, by setting $\alpha\neq0$ in (6)–(8). The most realistic situation represented by such trajectories is with $\delta=0$, discussed in Sec. V D (also see Fig. 8).

(6) *Point* D_3, *at* $(\pm\infty,\pm\infty)$, *representing* $|x|\to0$. Rewriting the governing equations in variables $\mu=1/U$ and $\nu=1/V$, we have, at leading order,

$$\frac{d\nu}{d\mu}=\left(\frac{\nu}{\mu}\right)\frac{(n+1)\nu-\mu}{2(\mu+\nu)}. \tag{12}$$

By introducing a variable $g=\nu/\mu$, (12) can be integrated: for $\mu>0$ it has the solutions

$$\begin{aligned} &n=0:\ (\nu/\mu^{3/2})(\nu+3\mu)^2=K;\\ &n=1:\ \nu/\mu+\log|\nu\mu^{1/2}|=K, \end{aligned} \tag{13}$$

where K is a constant. Suppose that $n=0$. If $K\neq0$, trajectories approach D_3 along curves $V\sim K^{1/3}|U|^{1/2}$ as $|U|\to\infty$, for $K>0$ in the first quadrant, and for $K<0$ in the second, provided they lie above a separatrix [the dotted line in Figs. 1(a) and 1(b)] that far from the origin is tangential to $U+3V=0$. Those beneath this curve approach D_{2-}. A similar pattern exists in ($U<0$): those above a separatrix parallel to $U+3V=0$ [not shown in Figs. 1(a) and 1(b)] approach D_{2+}, and otherwise approach D_3. It follows that trajectories reaching D_3 with $K\neq0$ represent $h\sim$const and $\Gamma\sim t^{(2\delta-1)}$ as $|x|\to0$. The two separatrices, on the other hand, for which $K=0$, represent solutions satisfying $h\sim$const and $\Gamma\sim x^{2/3}t^{4\delta/3-1}$ as $|x|\to0$. If $n=1$, then trajectories that approach the fixed point satisfy $V\sim2U/\log|U|\to\infty$, so again $h\sim$const and $\Gamma\sim t^{(2\delta-1)}$ as $|x|\to0$.

Finally, four fixed points lie on the line $V=2\delta$ (with $\delta>0$): C_1 at $(0,2\delta)$; C_2 at $(2\delta^2/[(2\delta-1)],2\delta)$; and C_3 at $(\pm\infty,2\delta)$. Only C_2 plays a significant role in the heteroclinic bifurcation at $n=0$, $\delta=1$, but it does not represent a physically meaningful limit.

V. RESULTS

A. Spreading monolayers

The solutions for a spreading monolayer "strip," "drop," and "front" described previously[5] are readily recovered. Each has three components [see Figs. 1(a)–1(c)]: the separatrix from A in $U>0$, representing the monolayer in $0<x<t^\delta$; the trajectory AO, representing the shock; and the fixed point O, representing the uniform state ahead of the shock, $h=1$ (say) and $\Gamma=0$ for $x>t^\delta$. The strip solution, for which $n=0$, $\delta=\frac{1}{3}$, corresponds to the trajectory $U>0$, $V=\frac{1}{3}$ in Fig. 1(b). Substituting this value of V into (6a) and (8), the solution,

$$h=\frac{2x}{t^{1/3}},\quad \Gamma=\frac{1}{6t^{1/3}}\left(1-\frac{x}{t^{1/3}}\right),\quad \text{for } 0<x\leqslant t^{1/3}, \tag{14}$$

is easily found. Note that the magnitude of the jump in film height from $h=2$ to $h=1$ at the shock cannot be determined by this method: the governing equations must be integrated directly. Similarly, for the drop solution, with $n=1$ and $\delta=\frac{1}{4}$, the line $V=\frac{1}{4}$ is a trajectory [Fig. 1(c)], and the corresponding solution for the region upstream of the shock is

$$h(x,t)=2\left(\frac{x}{t^{1/4}}\right)^2,\quad \Gamma(x,t)=-\frac{1}{8t^{1/2}}\log\left(\frac{x}{t^{1/4}}\right),$$
$$\text{for } 0<x\leqslant t^{1/4}. \tag{15}$$

These two exact solutions belong to a more general class of solutions for which α need not be zero, corresponding to $U>0$, $V=\delta$, $\delta=(1-\alpha)/[1+n+2(1-\alpha)]$. Numerical solutions of the full time-dependent equations (1) have shown that the unphysical behavior displayed by (14) and (15) at $x=0$ is not observed.[5] Instead, the solutions adjust to realistic boundary conditions over a diminishing boundary layer centered at $x=0$; this boundary layer has width $t^{1/6}$ for the strip and $t^{1/8}$ for the drop. Further, the effects of surface diffusion of surfactant,[1,2] capillary forces, or gravity,[2] however weak, will eliminate the discontinuity in h at the shock; for a detailed discussion of their effects see Ref. 5. So, even though solutions such as (14) or (15) violate the assumptions underlying the long-wavelength approximation at the shock, and are unphysical at the origin, they are still accurate approximations elsewhere in their domains.

The front solution, with $n=0$ and $\delta=\frac{1}{2}$, is represented by the trajectory B_+AO in Fig. 1(a). It must be determined numerically, and is shown as the solid line in Fig. 2. Although trajectories spiral around B_+, the physical solution does not exhibit this oscillatory character as $x\to0$. Again, $h=1$ and $\Gamma=0$ ahead of the shock, in $x>t^{1/2}$. This solution approximates the majority of the flow corresponding to a monolayer fed from a source $\Gamma=$const, advancing

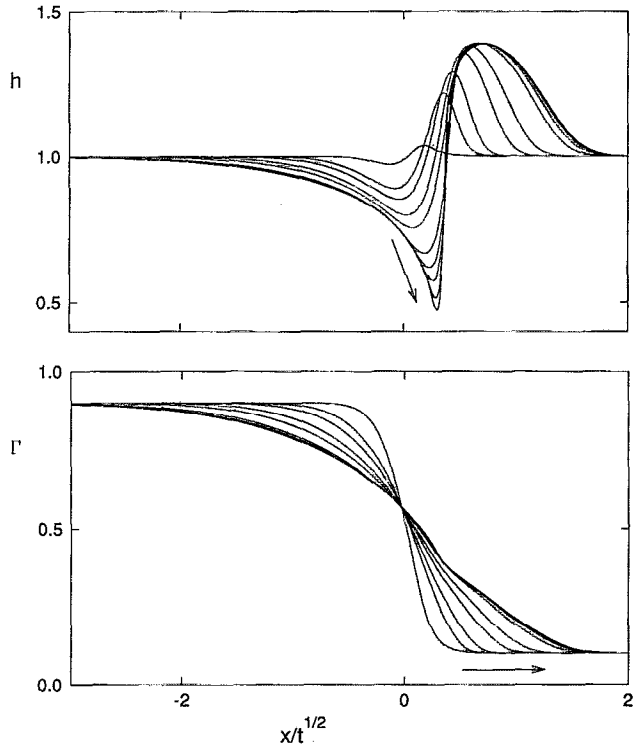

FIG. 3. A numerical solution of the breaking-dam problem, plotted in the $x/t^{1/2}$-frame at times $t=1.01$, 1.1, 1.2, 1.5, 2, 5, 10, 20, 50, and 100. Arrows indicate increasing time. The computational domain extends from $x/t^{1/2}=-6$ to $x/t^{1/2}=3$.

over an uncontaminated film, although once again numerical solutions of (1) deviate from the similarity solution as $x\to 0$.[5] Recall from Sec. IV that for $\delta=\frac{1}{2}$, all the trajectories arriving at O in Fig. 1(a) satisfy $\Gamma\sim$const as $x\to\infty$. These trajectories can either originate from B_+, D_+, D_3, or D_{2-}, the last case corresponding to flow off a plate lying in $x\geqslant t^{1/2}$. Examples of B_+O solutions are shown in Fig. 2. These are asymptotic approximations to the behavior of a monolayer fed from a source of constant concentration at $x=0$, spreading over a film on which there is an existing uniform surfactant concentration. The preexisting surfactant destroys the shock, and smooths the surfactant distributions.[5,11]

These trajectories all form part of a family of solutions that are closely related to the problem of the flow of a viscous gravity current after the breaking of a dam.[13] Suppose for $t<0$ a plane barrier at $x=0$ separates two monolayers of different, uniform concentrations, and that the barrier is removed at $t=0$. We assume that the more concentrated monolayer lies initially in $x<0$. A numerical solution of (1) including weak surface diffusion $D=0.005$ [represented as a term $x^{-n}(Dx^n\Gamma_x)_x$ on the right-hand side of the surfactant transport equation] is shown in Fig. 3. A finite difference scheme was used, based upon that developed in earlier studies;[5–7] the initial condition was a smooth Γ distribution, with Γ taking the values 0.9 and 0.1 far upstream and far downstream, respectively. The governing equations were solved, and are plotted, in the similarity frame, where $x/t^{1/2}$ is the independent spatial variable. A flow is generated in the x direction that perpetually reduces the gradient in surfactant concentration, in which fluid is drawn from $x<0$ into $x>0$. This results in thinning of the film in $x<Ct^{1/2}$, where $C\approx 0.3$, and an elevation of the film ahead of this. Figure 3 demonstrates that as time increases, the h and Γ distributions asymptotically approach a self-similar state over the majority of the domain, although for $0<x<Ct^{1/2}$ the rapid thinning of the flow remains unsteady in the self-similar frame. The flow in $x<0$ is represented by a trajectory in $U>0$, $V<0$, connecting D_3 and O in Fig. 1(a) (lying between $V=0$ and the dotted trajectory); the flow in $x>0$ is represented by a trajectory connecting B_+ and O. There is thus a correspondence between all such pairs of trajectories in Fig. 1(a): the limiting cases are the separatrix $D_{1+}O$, representing uniform h and Γ, and the pair of trajectories B_+AO (the "front" solution) and the separatrix D_3O [shown by the dotted line in Fig. 1(a)]. Note that in the latter case, $\Gamma\sim(x^2/t)^{1/3}$ as $x\to 0-$ rather than $\Gamma\sim$const [Sec. IV, Part 6].

B. Traveling wave solutions

The parameter values $n=0$, $\delta=1$ are exceptional, because there exists a heteroclinic trajectory connecting the saddle points A and O in $U<0$ *and* A and C_2 in $U>0$, given by $U=V(V-1)$. Its segment in $U<0$ combined with OA corresponds to the solution found by Borgas and Grotberg,[1] describing a monolayer being pushed along at constant speed:

$$h=\begin{cases}2, & \text{if } x<t\\ 1, & \text{if } x>t,\end{cases}\qquad \Gamma=\begin{cases}\frac{1}{2}(t-x), & x<t.\\ 0, & \text{if } x>t.\end{cases} \tag{16}$$

This is a member of a set of solutions for which $h\to 1$ and $\Gamma\to\Gamma_0$ as $x-t\to\infty$, given by

$$\log(h-1)+\frac{4}{2-h}=\frac{\xi_0-\xi}{\Gamma_0},$$

$$\text{with}\quad \frac{\Gamma}{\Gamma_0}=\frac{h}{2-h},\quad \xi=x-t. \tag{17}$$

Although (17) reduces to (16) in the limit $\Gamma_0\to 0$, it is not of a form that can be represented in the similarity formulation of Sec. III. However, it resembles the solutions shown in Fig. 2 for which $\Gamma\to$const at $x\to\infty$, and indicates very clearly how the rate at which $h\to 1$ as $x-t\to\infty$ is controlled by the strength of the mean surfactant concentration Γ_0.

C. A closing axisymmetric hole in a monolayer

Suppose that an axisymmetric region of the film is initially surfactant-free (a "hole"), while the surrounding area is covered with a monolayer of (say) uniform concentration. When a barrier maintaining this configuration is removed, the surfactant generates a flow that reduces the radius of the hole. A shock is formed at the shrinking circular boundary between the hole and the surrounding monolayer. Just as the area of the hole is about to vanish, we might expect the influence of the initial configuration

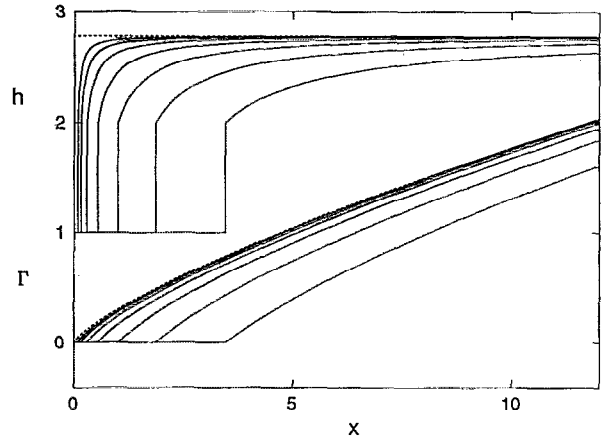

FIG. 4. The self-similar "closing-hole" solution, corresponding to the trajectory AO in Fig. 4, plotted at $t=-10^{2/3}$, $-10^{1/3}$, -1, $-10^{-1/3}$, $-10^{-2/3}$, -10^{-1}, and $-10^{-4/3}$. Curves move to the left as t increases. The dotted lines correspond to (18).

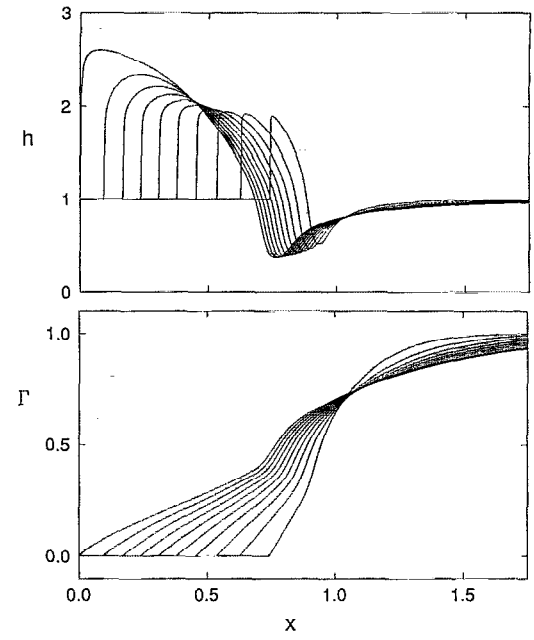

FIG. 5. A numerical solution of the closing-hole flow, computed by solving (1), including weak surface diffusion of surfactant with diffusivity $D=10^{-3}$. The film height and surfactant concentration are shown at ten equally spaced times between the initial condition at $t=1$ and the moment of closure $t_0=1.357$. Curves move to the left as t increases.

no longer to be significant in the neighborhood of the shock. This flow is analogous to the closing of a circular dry region in a thin viscous layer of fluid under the effects of gravity, as described in Ref. 11, which suggests that the closing-hole flow is also described by a similarity solution "of the second kind."

Because this is a flow in which the monolayer is contracting, we consider $t<0$, and seek suitable trajectories in $U<0$. The inwardly moving shock is represented by the trajectory OA on $U=0$. The monolayer outside the shock is represented by the separatrix that emerges from A. In general, this separatrix terminates either at B_- (or a limit cycle surrounding it), in which case $h\to 0$ as $x\to\infty$ [Sec. IV, Part 3], or at D_{2-}, in which case $h\to 0$ at the edge of a finite plate. However, for the exceptional case shown in Fig. 1(d), for which $n=1$ and $\delta=\delta_c\approx 0.807\,41$, this separatrix terminates at O, representing $h\sim$const as $x\to\infty$. These boundary conditions suggest that this heteroclinic trajectory will approximate the closing-hole flow.

We assume that within the hole, $h=1$ and $\Gamma=0$. The jump in film height at the shock must be from $h=1$ to $h=2$.[1] The solution corresponding to the trajectory AO in Fig. 1(d) can be determined numerically, and is shown in Fig. 4 for values of t approaching $0-$. (This solution was computed in two stages, integrating along the separatrix from A toward O with ϕ increasing, and then integrating from O toward A with ϕ decreasing, and patching the two solutions together.) Far from the shock [i.e., near O in the (U,V) plane], the solution is approximated by

$$h\sim 2.78, \quad \Gamma\sim 0.308x^{2-(1/\delta_c)}, \tag{18}$$

shown as dashed lines in Fig. 4. Because of the axisymmetric convergence of the flow, the film height exceeds the usual maximum possible height of 2. Furthermore, in the very final moments before the disappearance of the hole, (18) describes the complete monolayer distribution with the exception of a very small shrinking region near $x=0$.

Once the hole has vanished, an inward flow due to surface-tension gradients might persist for a short period, with a sharp spike of fluid growing at $x=0$, represented by the trajectory $D_{1+}O$ in $U>0$, $V<0$ in Fig. 1(d). This is highly unlikely to be observed in practice, however, because the massive curvature of the spike would mean that its development is soon dominated by restraining capillary effects. Furthermore, a sharp spike is unlikely to be described accurately by lubrication theory.

It is important to ascertain how these similarity solutions compare with solutions that satisfy physically realistic boundary conditions, and that are affected by effects such as surface diffusion. To do so, solutions of (1) were computed, including a very weak surface diffusion $D=0.001$ (a 2000-node finite difference grid over $0<x<3$ was used to resolve the shock in this case), and the results are shown in Fig. 5. The initial conditions used were a hole in a monolayer with the surfactant concentration varying smoothly at its boundary ($h=1$, $\Gamma=\frac{1}{2}\{1+\tanh[100(x-1)]\}$). As expected, an inwardly moving shock is formed; the shock is very weakly smoothed by surface diffusion, preventing the film height initially from reaching $h=2$. As the hole closes, however, the maximum film height exceeds $h=2$, as predicted, although the effects of diffusion are sufficiently strong to prevent it from attaining 2.78. The integration was terminated at the final possible stage with h and Γ still very close to 1 and 0, respectively, at $x=0$. The radius of the hole, $x_s(t)$, is shown as a function of t in Fig. 6. When plotted on a logarithmic scale, it is shown to be well approximated by $x_c\propto(t_0-t)^{\delta_c}$. The surfactant concentration, shown at the moment of closure in Fig. 7, is also close to the approximate distribution (18) over a significant portion of its length. It is only for $x>0.5$, say, that

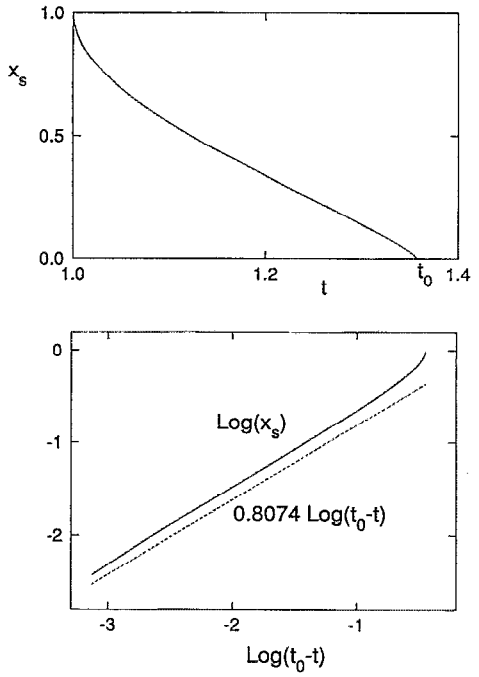

FIG. 6. The radius of the hole $x_s(t)$, plotted as a function of time and on a logarithmic scale for comparison with the self-similar prediction.

the influence of the initial conditions and the boundary conditions ($h\to 1$ and $\Gamma\to 1$ as $x\to\infty$) are evident.

An asymptotic estimate of the importance of diffusion and other effects is also revealing. Following exactly the approach used in Ref. 5, one can seek the scalings for the "inner" layer across which the shock is smoothed. Supposing that the shock lies at $(-t)^{\delta_c}$, and that the inner layer has width X, then appropriate inner variables are given by $x=(-t)^{\delta_c}+X\zeta$, $h(x,t)=H_i(\zeta,t)$ and $\Gamma(x,t)=X(-t)^{\delta_c-1}G_i(\zeta,t)$. Substituting this expansion into (1) (supplemented by a surface-diffusion term), the Marangoni and diffusive terms are of the same order provided $X=X_D=\mathscr{D}(-t)^{1-\delta_c}$, where $\mathscr{D}\ll 1$. Thus, diffusive effects at the shock are confined to a small, shrinking inner layer, provided $X_D\ll(-t)^{\delta}_c$, i.e., for

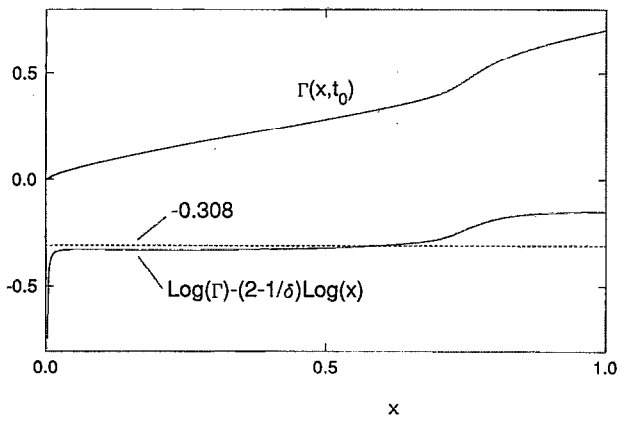

FIG. 7. Comparison of the numerical solution for $\Gamma(x,t_0)$, at the instant of closure of the hole, with the asymptotic solution (18).

$|t|\gg O(\mathscr{D}^{1/(2\delta_c-1)})$. Only at the very final moments of closure is the outer approximation in Fig. 4 clearly no longer going to be accurate. This is consistent with Fig. 5. Similarly, it is straightforward to show that capillary effects are confined to an inner layer that shrinks proportionately to $(-t)^{(1-\delta_c)/3}$, so again it is only at the very late stages of closure, when gradients in h have steepened sufficiently, that the asymptotic model in Fig. 4 will break down. These numerical and asymptotic results therefore demonstrate that the similarity solution shown in Fig. 4 is a good approximation of the closing-hole flow, albeit over a limited range of space and time.

D. Quasisteady solutions: $\delta=0$

Finally, in the case $\delta=0$ one recovers what might be called quasisteady solutions of (1), in which $\hat{h}$, $\hat{\Gamma}$, and $\hat{v}$ [see Eq. (3)] are all assumed to be functions of x alone, although h, Γ, and v retain the simple time dependence given by (2). These solutions therefore differ from completely steady surfactant-driven flows described previously (e.g., Ref. 10), but complement the example presented there of a surfactant-driven flow over a plate of finite extent. An example of such a solution is given here for the case $n=0$ and $\alpha=0$. In this case one can proceed directly from (3), without recourse to the phase plane; analogous solutions can readily be found for other values of these parameters, corresponding to different geometries or with various source strengths of fluid at $x=0$.

Defining $\tilde{h}=\hat{h}$, $\tilde{\Gamma}=x^2\hat{\Gamma}$, and $\tilde{v}=x\hat{v}$, (3) may be written as

$$(\tilde{h}\tilde{v})_x=0,\quad (\tilde{\Gamma}\tilde{v})_x-\tilde{\Gamma}=0,\quad \tilde{v}+\tilde{h}\tilde{\Gamma}_x=0. \tag{19}$$

Putting $\tilde{h}\tilde{v}=A=\text{const}$, and defining $w=\tilde{v}\tilde{\Gamma}$, it follows that $\tilde{\Gamma}=w_x$, $\tilde{v}=w/w_x$, and $Aw_{xx}(w_x)^2+w^2=0$. Letting $\eta(w)=w_x$, this last equation becomes $A\eta^3(d\eta/dw)+w^2=0$, which is easily integrated to give $\frac{1}{4}Aw_x^4+\frac{1}{3}w^3=B=\text{const}$. When $B=0$, the solution corresponds to an exact solution of (7), $4V^2+3U=0$. For $B\neq 0$, the two constants can be eliminated through rescaling w and x, and so, in general, solutions are governed by

$$w_x=(1-w^3)^{1/4}. \tag{20}$$

A numerical solution of (20) is shown in Fig. 8, corresponding a flow off a plate of unit width. In the neighborhood of the edge of the plate, as $x\to 1-$, $w\sim 1-[3^5 4^{-4}(1-x)^4]^{1/3}$, and so (ignoring constants) $h\sim(1-x)^{1/3}$, $\Gamma\sim t^{-1}(1-x)^{1/3}$, and $v\sim t^{-1}(1-x)^{-1/3}$. This solution is unlikely to be accurate where gradients in h are very large, but effects neglected here, such as surface diffusion, can be expected to remove the singular behavior at $x=1$.[10]

VI. CONCLUSIONS

The nonlinear evolution equations describing the behavior of a dilute insoluble surfactant monolayer on a thin liquid film (1) admit similarity solutions of the form given by (2) and (4). For a given geometry (specified by n), and given values of the parameters α and δ, these solutions may

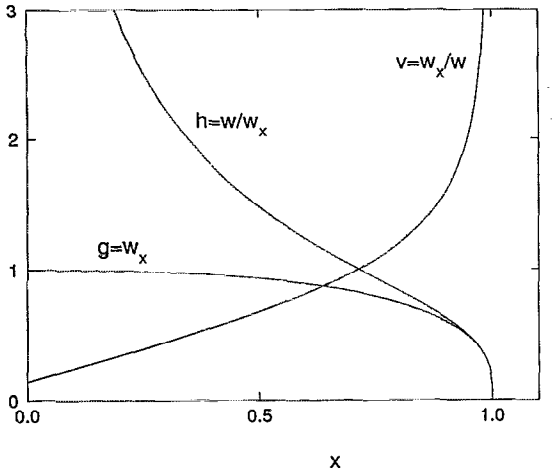

FIG. 8. A solution of (20), corresponding to drainage off a plate of unit width.

be represented by trajectories filling a two-dimensional phase plane. The nature of the corresponding physical solutions can be determined to a large extent by examining the asymptotic behavior of variables near the fixed points in the phase plane. All similarity solutions of the appropriate form can thereby be systematically examined, but because only some of the symmetries of (1) have been exploited, there presumably exist additional self-similar solutions that cannot be described by the techniques described in Sec. III. Some of the solutions presented here have been described previously, e.g., the spreading of localized surfactant distributions[1,5] (Secs. V A and V B), but this method reveals many new solutions, a small subset of which are of significant physical interest. A key feature of the governing equations is their similarity to a class of nonlinear diffusion equation, in particular, that which governs the evolution of a viscous gravity current, despite the fact that (1) involves a *pair* of coupled equations. Many solutions analogous to the gravity-current flows described in Ref. 11 can be found. These are either similarity solutions "of the first kind," e.g., the flow ensuing after a barrier is removed separating monolayers of different concentrations (Figs. 2 and 3), or the flow off a plate (Fig. 8), or, more significantly, a new similarity solution "of the second kind," representing the final stages in the closing of an axisymmetric hole in a monolayer (Figs. 4–7). The latter is an analog of "focusing" solutions of a class of nonlinear diffusion equations.[18]

The value of these solutions is that they act as useful approximations to a variety of realistic surfactant-driven flows, albeit generally over restricted ranges of space and time. Differences between the similarity solutions and realistic flows can arise, both because of differences between the self-similar solutions and fully time-dependent solutions of (1), and because of physical effects neglected in (1). Discrepancies can therefore be expected to occur in the following circumstances: at the early stages of the flow, as it adjusts from its initial conditions to self-similar form (e.g., Figs. 3, 5, and 6); at the boundaries of the flow, for example, near $x=0$ in Fig. 3, or as $x\to\infty$ in Fig. 7; at the shock, because the long-wavelength approximation is violated and because of the neglect of surface diffusion (demonstrated in Fig. 5), gravity, capillary forces, or inertia (which may be important in the very final stages of hole closure, once $\epsilon^2\,\mathrm{Re}\,\ddot{x}_s=O(1)$, i.e., for $t=O[(\epsilon^2\,\mathrm{Re})^{1/(2-\delta_c)}]$); and throughout the flow, again because of the neglect of these physical effects or because the surfactant is sufficiently concentrated for nonlinearities in its physicochemical properties to be important. Despite all these considerations, however, numerical results here and in Ref. 5 confirm that away from the shock, and from other boundaries over a suitable time interval, the similarity solutions provide valuable approximate solutions. This was confirmed numerically here for the approximation of a closing hole in a monolayer (Figs. 4 and 8), but remains to be verified experimentally.

One class of solutions presented here has important applications to the delivery of surfactants to the lung. As artificial (exogenous) surfactant spreads over the liquid lining of the lung airways, it will, in general, encounter existing concentrations of natural (endogenous) lung surfactant.[11] The self-similar solutions presented in Fig. 2, and the analytic solution (17), show how the endogenous surfactant destroys the shock that would otherwise exist at the monolayer's leading edge, but at the same time lengthens the proportion of the domain influenced by the exogenous surfactant. The manner in which a solute (e.g., a drug) dissolved in the fluid layer is transported by such flows is currently being investigated.[19]

This method can also be extended to non-Newtonian fluids for which the stress–strain relation satisfies a power-law relation. In this case, the surface-velocity expression in Eq. (1) can be replaced by $v+h(\Gamma_x)^\gamma=0$ for some constant γ, and a slightly modified form of the transformation in Sec. III can be used to describe a new set of phase planes governed by the additional parameter γ. This calculation might be appropriate to models of surfactant-driven flows over lung mucus, for example. Although mucus has very complex and highly variable rheology, one significant property it exhibits is shear thinning,[20] which would be represented by $\gamma>1$. It is easily shown, for example, that a spreading monolayer strip ($n=0$) or drop ($n=1$) of surfactant would then grow proportionally to $t^{1/[1+(n+2)\gamma]}$, quantifying very simply the degree to which shear thinning can influence spreading rates.

[1] M. S. Borgas and J. B. Grotberg, "Monolayer flow on a thin film," J. Fluid Mech. **193**, 151 (1988).
[2] D. P. Gaver III and J. B. Grotberg, "The dynamics of a localized surfactant on a thin film," J. Fluid Mech. **213**, 127 (1990).
[3] S. M. Troian, E. Herbolzheimer, and S. A. Safran, "Model for the fingering instability of spreading surfactant drops," Phys. Rev. Lett. **65**, 333 (1990).
[4] D. P. Gaver III and J. B. Grotberg, "Droplet spreading on a thin viscous film," J. Fluid Mech. **235**, 399 (1992).
[5] O. E. Jensen and J. B. Grotberg, "Insoluble surfactant spreading on a thin viscous film: shock evolution and film rupture," J. Fluid Mech. **240**, 259 (1993).
[6] O. E. Jensen and J. B. Grotberg, "The spreading of heat or soluble surfactant along a thin liquid film," Phys. Fluids A **5**, 58 (1993).

[7]D. Halpern and J. B. Grotberg, "Dynamics and transport of a localized soluble surfactant," J. Fluid Mech. **237**, 1 (1992).
[8]L. O. Kornum and H. K. Raaschou Nielsen, "Surface defects in drying paint films," Prog. Organic Coatings **8**, 275 (1980).
[9]S. B. G. M. O'Brien, "On Marangoni drying: Nonlinear kinematic waves in a thin film," J. Fluid Mech. **254**, 649 (1993).
[10]S. H. Davis, A-K. Liu, and G. R. Sealy, "Motion driven by surface-tension gradients in a tube lining," J. Fluid Mech. **62**, 737 (1974).
[11]F. F. Espinosa, A. H. Shapiro, J. J. Fredberg, and R. D. Kamm, "Spreading of a small surfactant bolus on a thin film lining an airway," J. Appl. Physiol. **75**, 2028 (1993).
[12]R. Courant and K. O. Friedrichs, *Supersonic Flow and Shock Waves* (Interscience, New York, 1948).
[13]J. Gratton and F. Minotti, "Self-similar viscous gravity currents: phase plane formalism," J. Fluid Mech. **210**, 155 (1990).
[14]J. A. Diez, R. Gratton, and J. Gratton, "Self-similar solution of the second kind for a convergent viscous gravity current," Phys. Fluids A **4**, 1148 (1992).
[15]D. G. Aronson, "The porous medium equation," in *Nonlinear Diffusion Problems*, Lecture Notes in Mathematics, No. 1224, edited by A. Dold and B. Eckmann (Springer-Verlag, New York, 1986).
[16]J. A. Diez, J. Gratton, and F. Minotti, "Self-similar solutions of the second kind of nonlinear diffusion-type equations," Q. J. Appl. Mech. L, 401 (1992).
[17]G. I. Barenblatt and Y. B. Zel'dovich, "Self-similar solutions as intermediate asymptotics," Annu. Rev. Fluid Mech. **4**, 285 (1972).
[18]D. G. Aronson and J. Graveleau, "A selfsimilar solution to the focusing problem for the porous medium equation," Eur. J. Appl. Math. **4**, 65 (1993).
[19]O. E. Jensen, D. Halpern, and J. B. Grotberg, "Transport of a passive solute by surfactant-driven flows." Chem. Eng. Sci. (in press).
[20]D. B. Yeates, "Mucus rheology," in *The Lung: Scientific Foundations*, edited by R. G. Crystal and J. B. West (Raven, New York, 1991).